

Fabrication of TiO₂ Nanostructures on Ti₃SiC₂ Substrate by Anodic Oxidation

Qin Hou, Hong-Feng Yin*, Hu-Die Yuan, Yun Tang, and Yan-Zhi Cai

College of Materials and Mineral Resources, Xi'an University of Architecture and Technology, Xi'an 710055, China

A TiO₂ nanostructure was prepared on a Ti₃SiC₂ substrate with different water and NH₄F concentrations in a fluoride-containing ethylene glycol electrolyte via an anodization process using the same constant-anodization potentials, anodization duration and temperature. The as-prepared samples were characterized by a field-emission scanning electron microscope equipped with an energy dispersive X-ray spectroscope, as well as by X-ray diffraction and X-ray photoelectron spectroscopy. The influence of the anodizing parameters and annealing temperature on the morphology of the nanostructure and the phase structure was studied. The results showed that the scattered TiO₂ nanotubes and TiO₂ nanoporous films were successfully fabricated in the glycol electrolyte containing (3.0 wt%) NH₄F + (5.0 vol%) H₂O. The as-prepared samples before calcination were amorphous and could transform to the anatase phase at temperatures higher than 500 °C. As the annealing temperature increased, the crystallization of the anatase phase was enhanced, and the rutile phase appeared at 600 °C. The as-prepared samples mainly consisted of oxides. Ti₂O₃ and SiO₂ oxides were present in addition to TiO₂.

Keywords: TiO₂, Ti₃SiC₂, Nanostructure, Anodic Oxidation.

1. INTRODUCTION

Nanostructured titania has various applications in dye-sensitized solar cells,^{1,2} hydrogen generation,³ photocatalysis,^{4,5} lithium-ion batteries,^{6,7} gas sensors,^{8,9} and biomedical devices¹⁰ owing to its unique properties such as large surface area, superior adsorption ability, good electrical transport, chemical stability, and nontoxicity. Compared to films based on other forms of titania, nanoporous TiO₂ films are of great interest because of the higher surface area.¹¹ Many techniques including template-based synthesis,¹² sol-gel method,¹³ hydrothermal method,¹⁴ and anodic oxidation,¹⁵ have been reported for the fabrication of nanoporous TiO₂ films. Zwilling and co-workers¹⁶ achieved uniform porous TiO₂ via anodic oxidation in an acidic, fluoride-based electrolyte on a Ti-based alloy substrate; subsequently, extensive efforts have been made to fabricate TiO₂ nanostructures by anodization. At the same time, much research has focused on the relation between the anodizing conditions and the nanotubes morphology, composition, properties and mechanism of anodic nanoporous oxide growth.

Among all the methods reported for producing nanoporous titania films, electrochemical anodization is the most widely used because it is simple, low cost, and gives reproducible results. In addition, it allows for control of the thickness and morphology, and facilitates the tuning of the size and shape of the films to the desired dimensions. Finally, this method fulfills the demands for specific applications because of controlled anodic oxidation of the metal substrate.^{17–19} Manea and co-workers²⁰ obtained nanoporous titanium oxide films via anodic oxidation on glass substrates; the films had a nanoporous structure with pore dimensions between 50 and 80 nm. Indira and co-workers²¹ reported the porous surface of titania films formed in aqueous (sulfuric acid) and neutral organic (glycerol) electrolytes containing different concentrations of HF by titanium anodization. They found that the average pore diameter and thickness of the porous layer depended on the electrolytes. Additionally, the as-prepared titania nanopores were amorphous, whereas heat treated titania nanopores were in the anatase phase. Hao and co-workers²² investigated the effects of the surface characteristics of nanoporous titanium oxide films formed on Ti-24Nb-4Zr-8Sn alloy by anodization in NH₄F solution, and found that nanoporous titanium

*Author to whom correspondence should be addressed.

oxide films have two different pore sizes (30 and 90 nm). Hou and co-workers²³ synthesized N-doped anatase TiO₂ nanoworm/nanotube hierarchical structures by immersion in hot ammonia solution. These hierarchical structures, with a larger surface area, higher electrical conductivity, and broader light absorption range than the original TiO₂ nanotubes arrays (TNAs), show dramatically enhanced photocatalytic activity for the degradation of methyl orange (MO) under visible light irradiation. Zhou and co-workers²⁴ prepared B, N co-doped nanotube arrays in an electrolyte containing BF₃ via an anodization process on a Ti sheet. The photocatalytic activity and photoelectrochemical properties of the nanotubes arrays were superior those of the TNAs. The synergistic effects of B and N co-doping were confirmed by photocatalytic and photoelectrochemical performances. Hua and co-workers²⁵ successfully synthesized highly ordered Fe, N, and F tri-doped TiO₂ (Fe, (N, F)-TiO₂) nanotube arrays by a facile one-step electrochemical anodization in an NH₄F electrolyte containing Fe ions leading to enhanced visible light photoactivity and higher stability.

MAX phases with the chemical formula M_{n+1}AX_n ($n = 1$ to 3; M is a transition metal (M = Ti, V, Cr, Zr, Nb, Mo, Hf, Ta and W); A is an A-group element (mostly IIIA and IVA); and X is C or N), as discovered by Nowotny,²⁶ are studied widely because of their unique combination of properties originating from both the metals and the ceramics. The layered ternary carbide Ti₃SiC₂ is one of the most common MAX phase that has attracted much interest because of its good physical and mechanical properties; low density; high Young's modulus; excellent electrical and thermal conductivity; good machinability; and high resistance to thermal shock, oxidation, and corrosion.^{27,28} In recent years, many researchers have studied Ti₃SiC₂ solid solutions or compounds using various elements such as V, Cr, Al, and Sn,^{29–33} so that TiO₂ nanostructure fabricated on a Ti₃SiC₂ substrate could be doped with other elements. Meanwhile, a Ti₃SiC₂ sheet showed higher electrical conductivity than did Ti as an anode. In this study, we designed and fabricated TiO₂ nanostructure on a Ti₃SiC₂ substrate in a fluoride-containing ethylene glycol electrolyte via an anodization process. The effects of water content and NH₄F concentration on the morphology of the TiO₂ nanostructure were studied. The influence of annealing temperature on the crystallization and phase transformation of anodized Ti₃SiC₂ samples also discussed.

2. EXPERIMENTAL DETAILS

2.1. Ti₃SiC₂ Preparation

TiC (average particle size: $\leq 2.6 \mu\text{m}$, purity >99.9%), Ti (average particle size: $\leq 45 \mu\text{m}$, purity >99.5%) and Si (average particle size: $\leq 45 \mu\text{m}$, purity >99.5%) powders were used as raw materials. These powders were mixed with a mole ratio of 2:1:1.2 and the mixtures were ball-milled in a 500 mL-polyurethane containers with

ethanol as the dispersion medium for 3 h. After milling and drying, the powders were compacted into a 44 mm diameter graphite mold whose inner surface was sprayed with boron nitride (BN). The compacted mixture was hot-pressed at 1500 °C for 3 h at a pressure of 25 MPa to fabricate dense Ti₃SiC₂ samples.

2.2. TiO₂ Nanostructure Preparation

The TiO₂ nanostructure was fabricated by an anodic oxidation method in a fluoride glycol electrolyte containing ethylene. All the chemicals were of analytical grade and were used without further purification. A Ti₃SiC₂ sheet was used as the anodes, while graphite as a cathode. For anodization, the Ti₃SiC₂ sheet was cut to a size of 5 × 15 × 20 mm area, then degreased in an ultrasonic cleaner with acetone and ethanol for 20 min, followed by rinsing with deionized water and drying. The anodization was performed at 15 ± 1 °C using a direct current (DC) power supply (IT6833, ITECH) with magnetic agitation. During anodization, the distance between the anode and cathode was maintained at about 5 cm and the current was recorded using digital multimeter (34464A, Agilent). After fabrication, the sample was ultrasonicated in ethanol and deionized water to remove the electrolytes, and then annealed in argon atmosphere 400 °C–600 °C for 2 h.

2.3. Sample Characterization

The surface morphology was observed using field-emission scanning electron microscope (FE-SEM, SU8010, Hitachi Company) equipped with an energy dispersive X-ray spectroscope (EDS). The phase composition of the samples was determined by powder X-ray diffraction (XRD, DMAX-2400, Rigaku) using a diffractometer with Cu K α radiation. To analyze the elemental composition and the oxidation state of the samples, X-ray photoelectron spectroscopy (XPS, Krato Axis Ultra DLD) was used. The binding energy (BE) of the XPS spectra was calibrated with reference to the C 1s peak at 284.6 eV.

3. RESULTS AND DISCUSSION

3.1. Effect of Water Content on the Nanostructure Morphology

Water is the most common polar solvent used in anodic oxidation to prepare TiO₂ nanomaterials. Water molecules play a crucial role in the preparation of TiO₂ nanomaterials in two aspects: diluting the electrolyte, and providing H⁺ and O²⁻. Figure 1 shows the FE-SEM images of the surface morphology of anodized Ti₃SiC₂ at 30 V for 12 h in 1.5 wt% NH₄F with different water contents. The first three images reveal that nanostructured film is formed, and that the diameter of the nanoholes decrease and the depth of the nanoholes increase with an increase in the water content. Highly ordered nanoporous arrays are obtained with an average nanopore diameter of

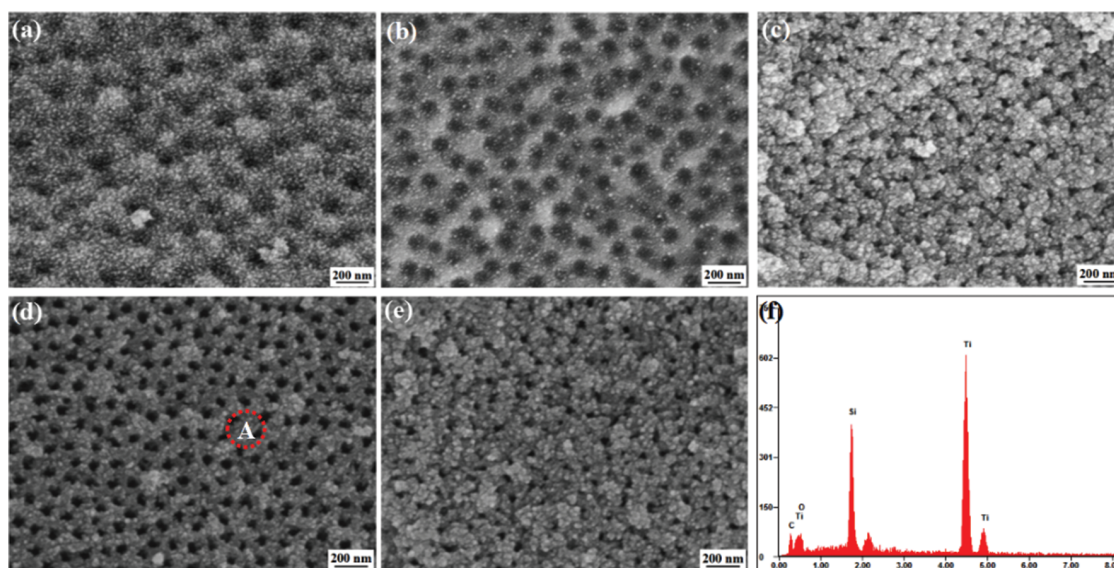


Figure 1. FE-SEM images of the anodized Ti₃SiC₂ at 30 V for 12 h in 1.5 wt% NH₄F with different water contents: (a) 2.0 vol%, (b) 3.0 vol%, (c) 4.0 vol%, (d) 5.0 vol%, (e) 6.0 vol%, (f) EDS of point A.

60 nm when the H₂O content increases to 5 vol%. However, the highly ordered nanoporous arrays become irregular again and there is a large amount of deposit formed on the nanoporous film surface when the H₂O content increases to 6 vol%. As described above, we can conclude that the viscosity of the electrolyte is reduced with an increase in the water content, so that the oxidation rate is accelerated. Meanwhile, more H⁺ and O²⁻ are provided for the formation of TiO₂ nanoporous arrays. Nevertheless, excessive water content accelerates the chemical dissolution rate of nanoporous arrays, resulting in a large amount of deposits on the top of the nanoporous arrays. EDS was used to determine the atomic composition of the nanoporous arrays (Fig. 1), revealing the presence of O. However, further characterization is necessary to understand the state of O.

3.2. Effect of NH₄F Concentration on the Nanostructure Morphology

The formation of nanotubes on the Ti substrate is a direct consequence of the competition between the rate of chemical dissolution of TiO₂ by fluoride etching and the rate of electrochemical formation.³⁴ According to the mechanism proposed by Macak and co-workers³⁵ the rate of chemical dissolution of TiO₂ nanotubes formed on a Ti substrate can be expected to increase with the NH₄F concentration, whilst the rate of electrochemical formation will either decrease with or be independent of the NH₄F concentration. Therefore, the NH₄F concentration plays a very important role in the formation and morphology of TiO₂ nanopores or nanotubes. Figure 2 shows the FE-SEM images of the surface morphology of anodized Ti₃SiC₂ at 30 V for 12 h in 5 vol% water with different NH₄F concentrations. At low concentrations, i.e., 1.5 wt%, 2.0 wt%, and

2.5 wt% NH₄F, the nanoporous films are regular, the average nanopore diameter increases, and there is little change in the nanopore diameter, where the tube walls are not formed. However, the surface density of the nanoporous array is gradually reduced at higher concentrations. At 3.0 wt% NH₄F, scattered nanotubes can be observed on the surface of the Ti₃SiC₂ substrate. An increase in the NH₄F concentration leads to a gradual dissolution of the titanium oxyfluoride film that binds the nanotubes walls, which gives rise to the formation of nanotubular films in electrolytes with 3.0 wt% NH₄F. At higher concentration, i.e., 3.5 wt% NH₄F, only a few nanotubes could be observed, and the highly ordered nanostructure becomes irregular again.

3.3. Effect of NH₄F Concentration on the Anodizing Current–Time Curves

Figure 3 shows the current–time curves of the anodized Ti₃SiC₂ at 30 V for 12 h in 5 vol% water with different NH₄F concentrations. It can be seen that at low concentrations, i.e., 1.5 wt%, 2.0 wt%, and 2.5 wt% NH₄F, the current initially dropped sharply, then increased slightly for several hours, and finally stabilized for the remaining anodization period. This kind of *I*–*t* behavior, where oxide formation and dissolution during anodization are competing processes, is similar to that previously reported by Liang and co-workers.³⁶ In the initial stage, a sharp decrease in the current is due to the formation of a compact oxide layer on the Ti₃SiC₂ substrate, which leads to a decrease in the surface conductivity. The subsequent slight increase in the current can be ascribed to the pitting of the compact oxide layer by the fluoride ions, which results in the localized decrease of the film thickness, re-oxidation of the Ti₃SiC₂ substrate, and random growth of the pores of

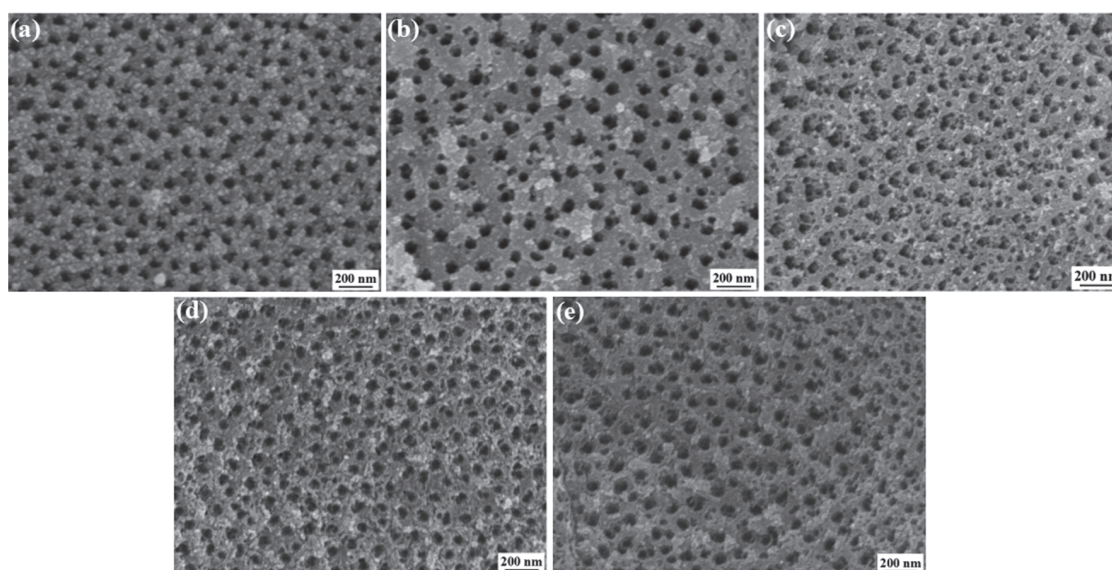


Figure 2. FE-SEM images of the anodized Ti₃SiC₂ at 30 V for 12 h in 5 vol% water with different NH₄F concentrations: (a) 1.5 wt%, (b) 2.0 wt%, (c) 2.5 wt%, (d) 3.0 wt%, (e) 3.5 wt%.

the oxide film. Lastly, self-assembled oxide nanopores are formed gradually, where the oxide formation rate is equal to that of its dissolution. Thereby, the current achieves a nearly steady-state value. However, the third stage of the *I*-*t* curve is distinct from the first three at higher concentrations. At 3.0 wt% NH₄F, the current is a wavy line over a small range. At higher concentration, i.e., 3.5 wt% NH₄F, the current continues increasing during the third stage. At 3.0 wt% NH₄F, formation and dissolution have been in a circulate state, leading to a gradual dissolution of the titanium oxyfluoride film that binds the nanotubes walls, so that scattered nanotubes could be observed as shown in Figure 2(d). In contrast, when the fluoride ion concentration is higher than 3.0 wt% NH₄F, the dissolution effect is more significant and the oxide formation rate is not equal to its dissolution, which results in a lower

regularity of the nanostructure as shown in Figure 2(e). Consequently, the current increases during oxidation. The inset in Figure 3 indicates that the peak current increases with the fluoride ion concentration. Similarly, higher fluoride ion concentration leads to higher constant current on the Ti₃SiC₂ substrate.

3.4. Crystal Structure Analysis

It is well known that TiO₂ nanomaterials obtained directly by anodization are amorphous and not photoactive.¹⁹ The crystal structure, composition, crystallite size, and crystallinity of TiO₂ have a significant influence on its properties. Therefore, it is necessary to transform the amorphous TiO₂ nanomaterials into the crystalline form for use in a wide range of applications.³⁷ Thermal treatment has been regarded as a facile route to induce crystallinity of the as-prepared TiO₂ nanomaterials, converting them into the anatase or rutile phase by adjusting experimental parameters such as temperature, time, and reaction atmosphere.^{38,39} XRD was used to analyze the changes in the crystal structure and phase transformation of the annealed TiO₂ samples. Figure 4 shows the XRD patterns of the anodized Ti₃SiC₂ samples annealed at different temperatures. The results show that the annealing temperature influences the crystallization and phase transformation of the as-prepared Ti₃SiC₂ samples to a certain extent. For samples annealed at 400 °C and 450 °C, apart from the Ti₃SiC₂ and TiC diffraction peaks from the substrate, no other diffraction peaks of TiO₂ were observed. With increasing annealing temperatures (from 500 °C to 600 °C), a small peak at $2\theta = 25.3^\circ$, corresponding to anatase TiO₂ can be observed. Meanwhile, at 600 °C, a small peak at $2\theta = 27.4^\circ$ corresponding to the diffraction peak of rutile TiO₂ appears, which indicates the phase

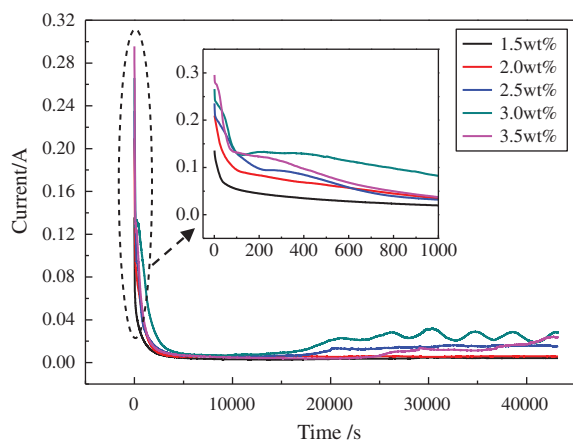


Figure 3. Current time curves of the anodized Ti₃SiC₂ at 30 V for 12 h in 5 vol% water with different NH₄F concentrations.

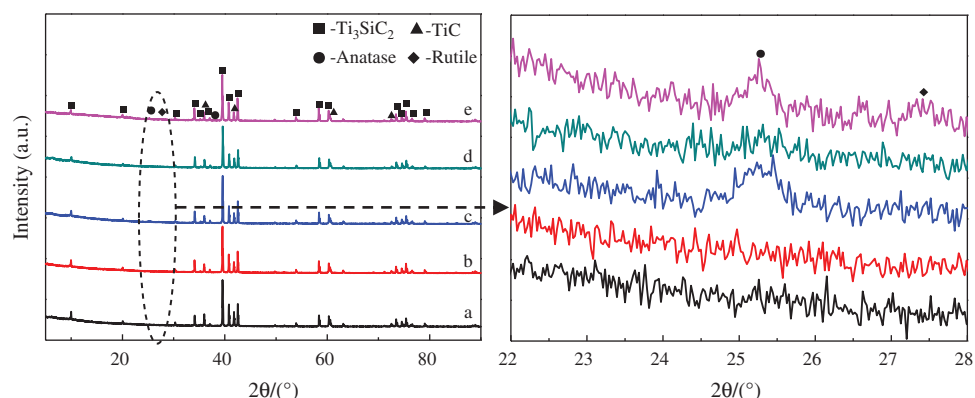


Figure 4. XRD patterns of the anodized Ti₃SiC₂ samples annealed at different temperatures in argon atmosphere for 2 h: (a) 400 °C, (b) 450 °C, (c) 500 °C, (d) 550 °C, (e) 600 °C.

transformation of anatase to rutile. However, peak intensities of anatase and rutile TiO₂ are both not obvious because of their low content. Although the content of the TiO₂ phase is low, it was proven that TiO₂ nanopores and nanotubes were formed.

3.5. Chemical Composition and Oxidation State Analysis

Chemical composition and the oxidation state of the anodized Ti₃SiC₂ samples were analyzed by XPS, and the deconvolution of the XPS peaks was performed using

Avantage 4.5.1 XPS software. Figure 5 shows the XPS spectra of the anodized Ti₃SiC₂ samples annealed at 600 °C in an argon atmosphere for 2 h. The XPS survey spectrum of the nanostructure, presented in Figure 5(a), indicates the presence of elemental C, Si, Ti, and O, whose atomic concentrations are 23.63 at.%, 13.13 at.%, 12.66 at.%, and 50.58 at.%, respectively. The atomic content of C is higher than Ti because of the introduction of hydrocarbon from the XPS measurement. Figure 5(b) shows the O 1s spectrum of the nanostructure, in which the O 1s core level peak is deconvoluted into two component

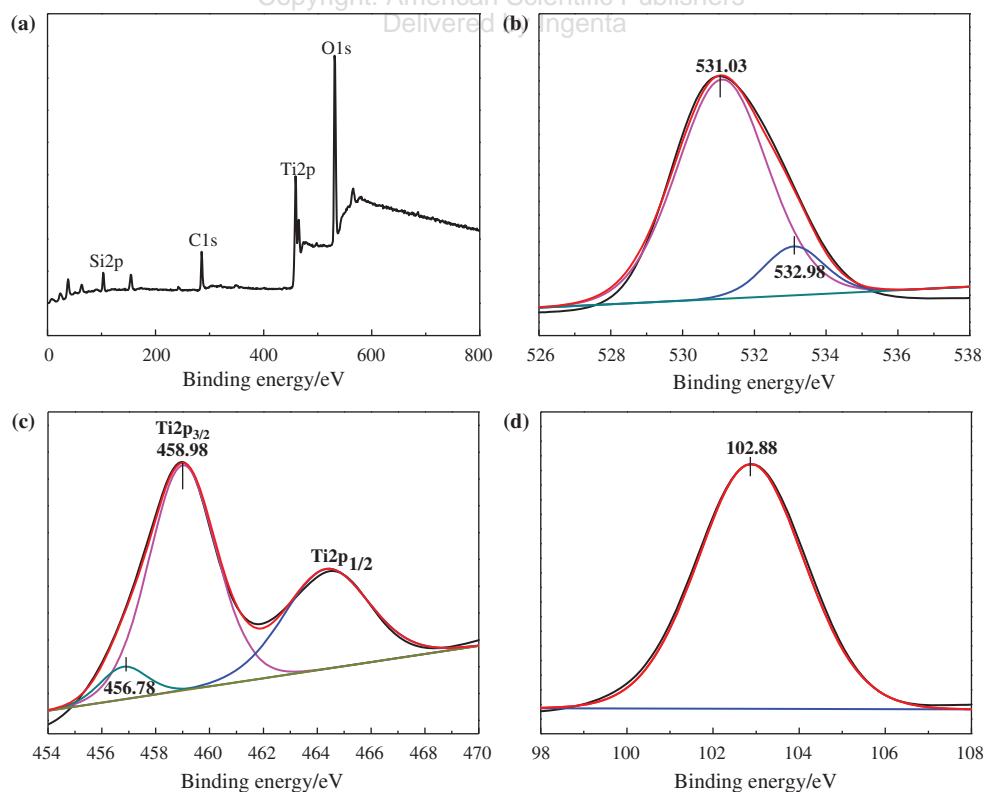


Figure 5. XPS spectra of the anodized Ti₃SiC₂ samples calcined at 600 °C in argon atmosphere for 2 h: (a) Survey spectrum, (b) O 1s, (c) Ti 2p, (d) Si 2p.

peaks at 531.03 and 532.98 eV. The lower binding energy O 1s peak at 531.03 eV was assigned to TiO₂, whereas the higher binding energy O 1s peak at 532.98 eV was assigned to SiO₂. The Ti 2p spectrum of the TiO₂ nanostructure, as shown in Figure 5(c), represents two typical Ti 2p_{3/2} and Ti 2p_{1/2} peaks. The Ti 2p_{3/2} core level peak is deconvoluted into two component peaks with binding energy at 456.78 and 458.98 eV, which is attribute to Ti³⁺ and Ti⁴⁺ oxidation state of Ti₂O₃ and TiO₂. Figure 5(d) shows the XPS spectrum of the Si 2p core level of the nanostructure. It can be observed that there is only a single peak at 102.88 eV, which is due to the SiO₂ incorporated in the TiO₂ nanostructure.

4. CONCLUSIONS

A TiO₂ nanostructure was prepared in a fluoride-containing ethylene glycol electrolyte via an anodization process on a Ti₃SiC₂ substrate by changing the electrolyte composition during anodization and subsequently annealing in argon atmosphere at different temperatures to crystallize it. The relationship between the morphology of the TiO₂ nanostructure and the anodizing parameters, including water content and NH₄F concentrations was studied. The effect of annealing temperature on the phase structure and the anatase-rutile phase transition was investigated. The obtained results showed that the scattered TiO₂ nanotubes and TiO₂ nanoporous films were successfully fabricated in the glycol electrolyte containing (3.0 wt%) NH₄F + (5.0 vol%) H₂O. The as-prepared samples before annealing were amorphous and could transform to the anatase phase at the temperature higher than 500 °C. As the annealing temperature increased, the crystallization of the anatase phase was enhanced and the rutile phase appeared at 600 °C. The as-prepared samples mainly consisted of oxide. In addition to TiO₂ oxide, Ti₂O₃ and SiO₂ oxides were present as well. The morphology and chemical composition of Ti₃SiC₂ and Ti oxidation are different.

Acknowledgments: The project supported by National Natural Science Foundation of China (Grant no. 51302206).

References and Notes

- H. Wang, Z. Guo, S. Wang, and W. Liu, *Thin Solid Films* 558, 1 (2014).
- M. N. An'amt, S. Radiman, N. M. Huang, M. A. Yarmo, N. P. Ariyanto, H. N. Lim, and M. R. Muhamad, *Ceram. Int.* 36, 2215 (2010).
- J. Gong, Y. Lai, and C. Lin, *Electrochim. Acta* 55, 4776 (2010).
- M. Nischk, P. Mazierski, M. Gazda, and A. Zaleska, *Appl. Catal. B Environ.* 144, 674 (2014).
- N. Liu, I. Paramasivam, M. Yang, and P. Schmuki, *J. Solid State Electrochem.* 16, 3499 (2012).
- N. Plylahan, M. Letiche, M. K. S. Barr, and T. Djenizian, *Electrochem. Commun.* 43, 121 (2014).
- R. Menéndez, P. Alvarez, C. Botas, F. Nacimiento, R. Alcántara, J. L. Tirado, and G. F. Ortiz, *J. Power Sources* 248, 886 (2014).
- P. M. Perillo and D. F. Rodríguez, *Sens. Actuators, B Chem.* 193, 263 (2014).
- Y. Gönüllü, A. A. Haidry, and B. Saruhan, *Sens. Actuators, B Chem.* 217, 78 (2014).
- D. Wei, W. Feng, Q. Du, R. Zhou, B. Li, Y. Wang, Y. Zhou, and D. Jia, *Ceram. Int.* 41, 13115 (2015).
- K. S. Raja, M. Misra, and K. Paramguru, *Electrochim. Acta* 51, 154 (2005).
- Y. Gao, M. Nagai, W. S. Seo, and K. Koumoto, *J. Am. Ceram. Soc.* 90, 831 (2007).
- Kartini, P. Meredith, X. S. Zhao, C. J. Da, and G. Q. Lu, *J. Nanosci. Nanotechnol.* 4, 270 (2004).
- T. Xu, H. Zheng, P. Zhang, W. Lin, and Y. Sekiguchi, *J. Mater. Chem. A* 3, 19115 (2015).
- G. D. Sulka, J. Kapusta-Kołodziej, A. Brzózka, and M. Jaskuła, *Electrochim. Acta* 55, 4359 (2010).
- V. Zwilling, M. Aucouturier, and E. Darque-Ceretti, *Electrochim. Acta* 45, 921 (1999).
- D. Yu, S. Zhang, X. Zhu, H. Ma, H. Han, and Y. Song, *J. Solid State Electrochem.* 18, 2609 (2014).
- Mazzarolo, M. Curioni, A. Vicenzo, P. Skeldon, and G. E. Thompson, *Electrochim. Acta* 75, 288 (2012).
- K. Indira, U. K. Mudali, T. Nishimura, and N. Rajendran, *J. Bio. Tribo. Corros.* 1, 1 (2015).
- E. Manea, C. Obreja, M. Purica, A. Dinescu, F. Comanescu, V. Schiopu, and E. Budianu, *J. Nano. Res.* 16, 113 (2012).
- K. Indira, S. Ningshen, U. K. Mudali, and N. Rajendran, *Mater. Charact.* 71, 58 (2012).
- Y. Hao, S. Li, X. Han, Y. Hao, and H. Ai, *Experimental and Therapeutic Medicine* 6, 241 (2013).
- X. Hou, C. W. Wang, W. D. Zhu, X. Q. Wang, Y. Li, J. Wang, J. B. Chen, T. Gan, H. Y. Hu, and F. Zhou, *Solid State Sci.* 29, 27 (2014).
- X. Zhou, F. Peng, H. Wang, H. Yu, and J. Yang, *Electrochem. Commun.* 13, 121 (2011).
- Z. Hua, Z. Dai, B. Xue, Z. Ye, H. Gu, and H. Xin, *J. Hazard. Mater.* 293, 112 (2015).
- V. H. Nowotny, *Prog. Solid State Chem.* 5, 27 (1971).
- M. W. Barsoum and T. El-Raghy, *J. Am. Ceram. Soc.* 79, 1953 (1996).
- M. W. Barsoum, *Prog. Solid State Chem.* 28, 201 (2000).
- B. Ghebouli, M. A. Ghebouli, M. Fatmi, L. Louail, T. Chihhi, and A. Bouhemadou, *Trans. Nonferrous Met. Soc. China* 25, 915 (2015).
- J. Emmerlich, P. Eklund, D. Rittrich, and H. H. L. Hultman, *J. Mater. Res.* 22, 2279 (2007).
- F. L. Meng, Y. C. Zhou, and J. Y. Wang, *Scripta Mater.* 53, 1369 (2005).
- K. Berndt, J. Engelmann, F. Storbeck, and G. Blasek, *Adv. Sci. Technol.* 45, 2648 (2006).
- C. Li, H. Zhai, Y. Ding, Y. Zhou, S. Li, and Z. Zhang, *Mater. Lett.* 61, 3575 (2007).
- Z. B. Xie and D. J. Blackwood, *Electrochim. Acta* 56, 905 (2010).
- J. M. Macac, H. Hildebrand, U. Marten-Jahns, and P. Schmuki, *J. Electroanal. Chem.* 621, 254 (2008).
- Y. Q. Liang, Z. D. Cui, S. L. Zhu, and X. J. Yang, *Thin Solid Films* 519, 5150 (2011).
- J. Yu and B. Wang, *Appl. Catal. B Environ.* 94, 295 (2010).
- L. Gang, Z. Q. Liu, L. Jing, W. Lei, and Z. Zhao, *Appl. Surf. Sci.* 255, 7323 (2009).
- M. Qamar, C. R. Yoon, H. J. Oh, D. H. Kim, J. H. Jho, K. S. Lee, W. J. Lee, H. G. Lee, and S. J. Kim, *Nanotechnology* 17, 5922 (2006).

Received: 28 September 2016. Accepted: 29 November 2016.